



# ALMA Lensing Cluster Survey: An ALMA Galaxy Signposting a MUSE Galaxy Group at $z = 4.3$ Behind “El Gordo”

K. I. Caputi<sup>1,2</sup>, G. B. Caminha<sup>1</sup>, S. Fujimoto<sup>2,3</sup>, K. Kohno<sup>4,5</sup>, F. Sun<sup>6</sup>, E. Egami<sup>6</sup>, S. Deshmukh<sup>1</sup>, F. Tang<sup>1</sup>, Y. Ao<sup>7,8</sup>, L. Bradley<sup>9</sup>, D. Coe<sup>9</sup>, D. Espada<sup>10</sup>, C. Grillo<sup>11,12,13</sup>, B. Hatsukade<sup>4</sup>, K. K. Knudsen<sup>14</sup>, M. M. Lee<sup>15</sup>, G. E. Magdis<sup>2,16,17</sup>, K. Morokuma-Matsui<sup>4</sup>, P. Oesch<sup>18</sup>, M. Ouchi<sup>19,20,21</sup>, P. Rosati<sup>22,23</sup>, H. Umehata<sup>24,25</sup>, F. Valentino<sup>2,3</sup>, E. Vanzella<sup>23</sup>, W.-H. Wang<sup>26</sup>, J. F. Wu<sup>9</sup>, and A. Zitrin<sup>27</sup>

<sup>1</sup> Kapteyn Astronomical Institute, University of Groningen, P.O. Box 800, 9700AV Groningen, The Netherlands; [karina@astro.rug.nl](mailto:karina@astro.rug.nl)

<sup>2</sup> Cosmic Dawn Center (DAWN), Copenhagen, Denmark

<sup>3</sup> Niels Bohr Institute, University of Copenhagen, Lyngbyvej 2, DK-2100, Copenhagen, Denmark

<sup>4</sup> Institute of Astronomy, Graduate School of Science, University of Tokyo, 2-21-1 Osawa, Mitaka, Tokyo 181-0015, Japan

<sup>5</sup> Research Center for the Early Universe, School of Science, The University of Tokyo, 7-3-1 Hongo, Bunkyo-ku, Tokyo 113-0033, Japan

<sup>6</sup> Steward Observatory, University of Arizona, 933 N. Cherry Avenue, Tucson, AZ 85721, USA

<sup>7</sup> Purple Mountain Observatory and Key Laboratory for Radio Astronomy, Chinese Academy of Sciences, Nanjing, People’s Republic of China

<sup>8</sup> School of Astronomy and Space Science, University of Science and Technology of China, Hefei, Anhui, People’s Republic of China

<sup>9</sup> Space Telescope Science Institute, 3700 San Martin Drive, Baltimore, MD 21218, USA

<sup>10</sup> SKA Organisation, Lower Withington, Macclesfield, Cheshire SK11 9DL, UK

<sup>11</sup> Dipartimento di Fisica, Università degli Studi di Milano, via Celoria 16, I-20133 Milano, Italy

<sup>12</sup> Dark Cosmology Centre, Niels Bohr Institute, University of Copenhagen, Lyngbyvej 2, DK-2100 Copenhagen, Denmark

<sup>13</sup> INAF—IASF Milano, via A. Corti 12, I-20133 Milano, Italy

<sup>14</sup> Department of Space, Earth and Environment, Chalmers University of Technology, Onsala Space Observatory, SE-43992 Onsala, Sweden

<sup>15</sup> Max-Planck-Institut für Extraterrestrische Physik (MPE), Giessenbachstr., D-85748 Garching, Germany

<sup>16</sup> DTU-Space, Technical University of Denmark, Elektrovej 327, DK-2800 Kgs. Lyngby, Denmark

<sup>17</sup> Niels Bohr Institute, University of Copenhagen, Lyngbyvej 2, DK-2100 Copenhagen Ø, Denmark

<sup>18</sup> Department of Astronomy, University of Geneva, Ch. des Maillettes 51, 1290 Versoix, Switzerland

<sup>19</sup> National Astronomical Observatory of Japan, 2-21-1 Osawa, Mitaka, Tokyo 181-8588, Japan

<sup>20</sup> Institute for Cosmic Ray Research, The University of Tokyo, 5-1-5 Kashiwanoha, Kashiwa, Chiba 277-8582, Japan

<sup>21</sup> Kavli Institute for the Physics and Mathematics of the Universe (Kavli IPMU, WPI), The University of Tokyo, 5-1-5 Kashiwanoha, Kashiwa, Chiba 277-8583, Japan

<sup>22</sup> Dipartimento di Fisica e Scienze della Terra, Università degli Studi di Ferrara, Via Saragat 1, I-44122 Ferrara, Italy

<sup>23</sup> INAF—Osservatorio di Astrofisica e Scienza dello Spazio, via Gobetti 93/3, I-40129 Bologna, Italy

<sup>24</sup> RIKEN Cluster for Pioneering Research, 2-1 Hirosawa, Wako-shi, Saitama 351-0198, Japan

<sup>25</sup> Institute of Astronomy, The University of Tokyo, 2-21-1 Osawa, Mitaka, Tokyo 181-0015, Japan

<sup>26</sup> Institute of Astronomy and Astrophysics, Academia Sinica, No. 1, Section 4, Roosevelt Road 11F of Astro-Math Building, Da-An District, Taipei 10617, Taiwan

<sup>27</sup> Department of Physics, Ben-Gurion University, Be’er-Sheva 84105, Israel

Received 2020 August 24; revised 2020 December 10; accepted 2020 December 16; published 2021 February 19

## Abstract

We report the discovery of a Multi Unit Spectroscopic Explorer (MUSE) galaxy group at  $z = 4.32$  lensed by the massive galaxy cluster ACT-CL J0102-4915 (aka El Gordo) at  $z = 0.87$ , associated with a 1.2 mm source that is at a  $2.07 \pm 0.88$  kpc projected distance from one of the group galaxies. Three images of the whole system appear in the image plane. The 1.2 mm source has been detected within the Atacama Large Millimetre/submillimetre Array (ALMA) Lensing Cluster Survey (ALCS). As this ALMA source is undetected at wavelengths  $\lambda < 2 \mu\text{m}$ , its redshift cannot be independently determined, however, the three lensing components indicate that it belongs to the same galaxy group at  $z = 4.32$ . The four members of the MUSE galaxy group have low to intermediate stellar masses ( $\sim 10^7$ – $10^{10} M_\odot$ ) and star formation rates (SFRs) of  $0.4$ – $24 M_\odot \text{yr}^{-1}$ , resulting in high specific SFRs (sSFRs) for two of them, which suggest that these galaxies are growing fast (with stellar mass doubling times of only  $\sim 2 \times 10^7$  yr). This high incidence of starburst galaxies is likely a consequence of interactions within the galaxy group, which is compact and has high velocity dispersion. Based on the magnification-corrected sub-/millimeter continuum flux density and estimated stellar mass, we infer that the ALMA source is classified as an ordinary ultra-luminous infrared galaxy (with associated dust-obscured SFR  $\sim 200$ – $300 M_\odot \text{yr}^{-1}$ ) and lies on the star formation main sequence. This reported case of an ALMA/MUSE group association suggests that some presumably isolated ALMA sources are in fact signposts of richer star-forming environments at high redshifts.

*Unified Astronomy Thesaurus concepts:* [High-redshift galaxies \(734\)](#); [Starburst galaxies \(1570\)](#); [Galaxy groups \(597\)](#); [Submillimeter astronomy \(1647\)](#)

## 1. Introduction

Lensing fields are excellent systems to study high-redshift galaxies to fainter limits than what is typically possible with current telescopes. Several observational campaigns (Postman et al. 2012; Lotz et al. 2017; Coe et al. 2019) have targeted lensing clusters with major observatories, such as the Hubble Space Telescope (HST), enabling a large number of studies of

the cluster members, as well as their magnified background sources.

The spectroscopic follow up of these background sources has proven especially useful to reveal the properties of faint galaxies up to redshift  $z \sim 6$ – $7$ . In addition to the study of pre-selected high- $z$  candidates, observations conducted with the Multi Unit Spectroscopic Explorer (MUSE) on the Very Large

Telescope (VLT) have allowed for significant serendipitous discoveries at high redshifts (e.g., Karman et al. 2015, 2017; Caminha et al. 2016; Vanzella et al. 2017b), including a few galaxy groups at redshifts  $z > 3$ . These galaxy groups have been found in association with diffuse Ly $\alpha$  nebulae or CIV absorption systems (e.g., Caminha et al. 2016; Vanzella et al. 2017a; Díaz et al. 2020). Here, we report the discovery of a group of Ly $\alpha$  emitters/absorbers at  $z = 4.3$  in association with an Atacama Large Millimetre/submillimetre Array (ALMA) sub-millimeter source.

For a long time, it has been considered that sub-/millimeter sources could trace active sites with multiple star-forming galaxies (e.g., Chapman et al. 2009; Martinache et al. 2018). To date, this idea has been mainly supported by the discovery of galaxy groups and proto-clusters dominated by bright sub-millimeter galaxies (Riechers et al. 2014; Umehata et al. 2015; Miller et al. 2018; Oteo et al. 2018). Some studies have reported cases of intrinsically fainter sub-millimeter sources whose flux densities are significantly boosted by gravitational lensing and belong to galaxy groups up to  $z \sim 3$  (e.g., Borys et al. 2004; Kneib et al. 2004; Garrett et al. 2005; Berciano Alba et al. 2007; MacKenzie et al. 2014). The system that we study here constitutes another example of this kind, albeit at a higher redshift  $z = 4.32$ .

Studying the properties of member galaxies in these mixed groups with sub-/millimeter sources and Ly $\alpha$  emitters/absorbers can help understand the consequences of close galaxy interactions. The majority of star-forming galaxies at different redshifts are located in the so-called star formation main sequence (e.g., Noeske et al. 2007; Speagle et al. 2014; Bisigello et al. 2018) on the star formation rate (SFR) versus stellar mass  $M^*$  plane. The fraction of starburst galaxies, i.e., galaxies with significantly enhanced star formation activity with respect to their past average SFR, is known to vary with stellar mass and redshift (e.g., Rodighiero et al. 2011; Sargent et al. 2012; Caputi et al. 2017; Bisigello et al. 2018). In any case, they range between a few and  $\sim 15\%$  of all known galaxies up to  $z \sim 5$ . This relative importance between main-sequence and starburst galaxies might be different in galaxy groups, where galaxy interactions could favor starburst episodes, but this is still poorly understood. The galaxy group that we study here allows us to investigate the importance of starbursts within compact galaxy groups at high redshifts.

Throughout this paper we adopt a cosmology with  $H_0 = 70 \text{ km s}^{-1} \text{ Mpc}^{-1}$ ,  $\Omega_M = 0.3$  and  $\Omega_\Lambda = 0.7$ . All magnitudes in this paper are total and are expressed in the AB system (Oke & Gunn 1983). Stellar masses and SFRs refer to a Chabrier (2003) initial mass function.

## 2. Data Sets

Our study is based on the analysis of the publicly available MUSE data for the massive galaxy cluster ACT-CL J0102-4915 (aka El Gordo) at  $z = 0.87$ . El Gordo is a well-studied galaxy cluster, whose total mass is estimated to be a few  $\times 10^{15} M_\odot$  (Menanteau et al. 2012; Zitrin et al. 2013; Cerny et al. 2018). The MUSE data on ACT-CL J0102-4915 was taken under the ESO program ID 0102.A-0266 (P.I. G. B. Caminha) and have a final depth of  $\approx 2.3$  hours on target using the GALACSI adaptive optics system. The data was processed using the reduction pipeline version 2.6 (Weilbacher et al. 2014), following all standard corrections and calibrations to create the stacked data cube. The final data covers the

wavelength range  $4700 \text{ \AA} - 9350 \text{ \AA}$  and the measured point-spread function full width at half maximum (FWHM) on the white images is  $\approx 0''.7$ . The detailed description of the data will be presented in Caminha et al. (2021).

The ALMA Band-6 (1.1–1.4 mm) data for El Gordo has been obtained as part of the ALMA Lensing Cluster Survey (ALCS) Large Programme (ID 2018.1.00035.L; P.I. K. Kohno), which has been carried out in ALMA’s cycles 6 and 7. The data have been reduced with the scripts provided by the ALMA observatory, using CASA versions 5.4.0 and 5.6.1 for cycles 6 and 7 data, respectively, following the standard pipeline.

The natural-weighted continuum map achieves a sensitivity of  $71.9 \mu\text{Jy/beam}$  and a synthesized beam size (FWHM) of  $1''.17 \times 0''.91$ . The details of the ALCS program description and the data reduction and imaging are presented in K. Kohno et al. (2020, in preparation) and S. Fujimoto et al. (2020, in preparation), respectively.

We note that the three components of the ALCS lensed source that we discuss here have also been detected in an earlier ALMA program (P.I. A. Baker) and reported as three different sources (Wu et al. 2018).

Finally, for the analysis of the ALMA source we also made use of Herschel Space Telescope Spectral and Photometric Imaging Receiver (SPIRE) data (Griffin et al. 2010), obtained as a part of the Herschel Lensing Survey (HLS; Egami et al. 2010) at a relatively shallow depth (rms =  $11.8 \text{ mJy beam}^{-1}$  at  $250 \mu\text{m}$ ). The data were reduced with the standard reduction pipeline described in Rawle et al. (2016). We extracted the SPIRE flux densities of the ALCS sources using an iterative point-spread-function fitting algorithm based on ALMA positional priors (F. Sun et al. 2020, in preparation).

## 3. An ALMA Bright Galaxy within a Lensed MUSE Galaxy Group at $z = 4.32$

### 3.1. System Description

The MUSE data clearly shows the presence of a group of four galaxies (ID #1 to #4) at  $z_{\text{spec}} = 4.32 - 4.33$ , which is triply lensed (Figure 1). The lensing model used in this paper, which is based on a large number of spectroscopically confirmed multiple images, will be presented in a companion paper (Caminha et al. 2021). As derived from this model, all these group galaxies are found within a physical distance of 30 kpc (in the source plane). In addition, another galaxy pair (ID #5 and #6), with no multiple images, is found behind El Gordo at  $z = 4.32$ , but is about 300 kpc away of the other, four-member galaxy group (which we call “main group” hereafter). Their connection to the main group is plausible, but not secure, so we will not discuss it further here. The coordinates and properties of all these sources are listed in Table 1.

Zitrin et al. (2013) and Diego et al. (2020) have previously identified a few of these multiply lensed galaxies from HST data, but had no spectroscopic redshifts for them. Nevertheless, their reported photometric/lensing-model redshifts were very close to our spectroscopic determinations.

Two galaxies in the main group (ID #1 and #3) have Ly $\alpha$  in emission, with a clear P-Cygni profile, according to the MUSE spectra (Figure 2). The signal-to-noise (S/N) ratio of the spectra is high enough to enable the detection of rest-UV absorption lines, such as CII  $\lambda$  1335, SiII  $\lambda$  1526, and CIV  $\lambda\lambda$  1548, 1551.

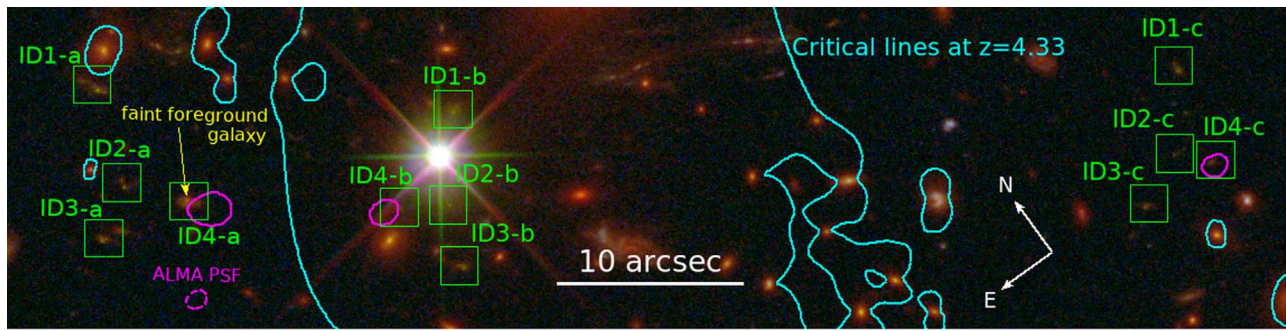


**Figure 1.** HST color image showing the three lensed images of the MUSE/ALMA galaxy group at  $z = 4.32$  behind the massive galaxy cluster El Gordo at  $z = 0.87$  (green squares). The regions with ALMA continuum emission (corresponding to the three images of the ALMA source) are delimited with magenta solid lines, while the ALMA beam size is indicated with a magenta dashed-line contour. The critical lines from the strong-lensing best-fit model at  $z = 4.33$  are also shown (cyan contours). The sources labeled as #5 and #6 in Table 1 are out of the field shown in this figure.

Source ID #4, instead, shows  $\text{Ly}\alpha$  only in absorption (Figure 2), with a very prominent Lyman break. Several other UV rest absorption lines are also clearly identified. For source ID #2, the  $\text{Ly}\alpha$  line is contaminated by a sky line, so it is unclear whether it has an emission component. Nonetheless, the continuum break, as well as some UV absorption lines (CII, SII), are evident and allowed us to safely determine the galaxy spectroscopic redshift.

The spectroscopic redshifts of the different MUSE galaxies (ID #1 to #4) allow us to estimate the rest-frame group velocity dispersion. We obtained  $\sigma_r \approx 300 \pm 160$  km/s, which indicates that this is likely an unrelaxed galaxy group (although, strictly speaking, the term “unrelaxed” refers to non-Gaussian radial velocity distributions, which cannot be determined for our galaxy group with only four members).

Independently, we found an ALMA Band 6 source that is associated with the MUSE source ID #4 (Figure 3). The total measured ALMA 1.2 mm flux densities are  $S_\nu(1.2 \text{ mm}) = 9.50 \pm 0.12$ ,  $3.83 \pm 0.11$  and  $3.29 \pm 0.12$  mJy, in the components a, b and c, respectively, making it a very secure detection in all cases. The ALMA source has been detected with the Spitzer Infrared Array Camera (IRAC; Fazio et al. 2004), but is detected neither with MUSE nor HST (it has a color  $F160W-[4.5] > 4$ ).

The ALMA source redshift can be obtained through the lensing-model analysis (Caminha et al. 2021). Its lensing-derived redshift is  $z_{\text{lens}} = 4.32^{+0.08}_{-0.06}$  (Figure 4), which indicates that the ALMA source is very likely part of the same galaxy group as the MUSE sources. In particular, the angular separation between the ALMA source and MUSE ID #4 implies that these sources are at a projected distance of  $2.07 \pm 0.88$  kpc in the source plane, which suggests that they might be two regions of the same galaxy. Indeed, other authors have reported intrinsic offsets of about 0.4 arcsec between the rest-frame UV and FIR emitting regions of a same galaxy (e.g., Chen et al. 2015), and these offsets can lead to separations of more than 1 arcsec in the image plane (Fujimoto et al. 2016). Nevertheless, we will analyze these two sources separately throughout this paper and discuss further the implications of being the same galaxy in Section 4.

### 3.2. Properties of the Group Galaxies

#### 3.2.1. The Lensed MUSE Sources

We performed the optical/near-IR spectral energy distribution (SED) fitting of all the MUSE sources of the main group

(sources ID #1 to #4) at their fixed spectroscopic redshifts, in order to recover their main properties (Figure 5). For this, we made use of the SED fitting code LEPHARE (Arnouts et al. 1999; Ilbert et al. 2006). We considered Bruzual & Charlot (2003) templates corresponding to a single stellar population and different exponentially declining star formation histories (SFHs), both with solar ( $Z_\odot$ ) and sub-solar ( $0.2 Z_\odot$ ) metallicities. To account for dust extinction we convolved the templates with the Calzetti et al. (2000) reddening law for different extinction values from  $E(B - V) = 0$  to 1.

We applied the SED fitting over 11 HST broad bands for sources in the components a and c, except for source ID #1a because its photometry is contaminated by a foreground-cluster member. The system component b is also close to cluster member galaxies, and thus the photometry is substantially contaminated for most sources (except for object ID #3b). We only incorporated IRAC photometry for source #3 (a,c), as only for this object is the IRAC photometry not significantly blended. This source shows a clear IRAC flux excess at  $3.6 \mu\text{m}$ , indicative of prominent  $\text{H}\alpha$  emission at its redshift (e.g., Caputi et al. 2017). Taking this into account, we checked the SED fitting with both IRAC bands and only  $4.5 \mu\text{m}$  in addition to the HST bands, and found that the results were consistent (we ran LEPHARE with emission lines, so the code can “recognize” the presence of  $\text{H}\alpha$ ).

The SED best fitting results indicate that source ID #1 has a preference for a solar metallicity template, while sources ID #2 and #3 have best-fit solutions with sub-solar metallicities. The output is less clear for source ID #4, which has best solution with solar metallicity in component a, while prefers a  $0.2 Z_\odot$  in component c. This might indicate that the true metallicity of this source is intermediate between  $0.2 Z_\odot$  and  $Z_\odot$ . All sources except source ID #4 have very low or no internal extinction. Even for source ID #4 the extinction is modest, with  $A_V < 1$  mag. This non-negligible extinction can explain why this source is the only one in the group with confirmed  $\text{Ly}\alpha$  in absorption and the most prominent Lyman break among our group sources.

LEPHARE’s output also provides us with stellar mass estimates (Table 1). The values derived for sources ID #2 and #3 are consistent within the error bars for the three different lensed components. Instead, the stellar mass of source ID #4 appears more loosely constrained, with a value between  $\sim 10^9$  and  $\sim 4 \times 10^{10} M_\odot$ , but in any case it is one of the most massive galaxies of our group.

**Table 1**  
List of MUSE Sources Belonging to the Galaxy Group at  $z \approx 4.32$  in Their Three Lensed Components

ID	$z_{\text{spec}}$	R.A.	Decl.	Ly $\alpha$	$M_*$ ( $\times 10^9 M_\odot$ )	SFR ( $M_\odot \text{ yr}^{-1}$ )	sSFR ( $\times 10^{-9} \text{ yr}^{-1}$ )	$\mu \pm 68\% \text{ CL}$
1a	4.3278	15.7324575	-49.2500982	E	...	...	...	$10.50_{-1.62}^{+2.53}$
2a	4.3175	15.7332889	-49.2514950	A? <sup>b</sup>	$0.02 \pm 0.01$	$1.06 \pm 0.24$	$53.0 \pm 28.6$	$5.64_{-0.34}^{+0.36}$
3a	4.3275	15.7343748	-49.2519405	E	$3.18 \pm 1.48$	$3.70 \pm 0.79$	$1.17 \pm 0.59$	$5.19_{-0.29}^{+0.30}$
4a	4.3196	15.7323007	-49.2522379	A	$40.1_{-36.7}^{+65.3}$	$23.48 \pm 2.14$	$0.59 \pm 0.75$	$8.25_{-0.59}^{+0.63}$
ALMA-a	...	15.7320058	-49.2525287	...	$77.7_{-49.4}^{+390.1}$	$221 \pm 93$	$2.84_{-2.57}^{+8.26}$	$9.77_{-0.73}^{+0.79}$
5 <sup>a</sup>	4.3181	15.7580432	-49.2739080	E	...	...	...	$4.80_{-0.21}^{+0.18}$
6 <sup>a</sup>	4.3187	15.7623243	-49.2800099	E	...	...	...	$23.99_{-14.67}^{+53.56}$
1b	4.3273	15.7262164	-49.2534759	E	...	...	...	$4.19_{-0.25}^{+0.26}$
2b	...	15.7275328	-49.2545678	A? <sup>b</sup>	...	...	...	$5.60_{-0.33}^{+0.36}$
3b	4.3269	15.7281160	-49.2554323	E	$1.76 \pm 0.49$	$2.20 \pm 0.48$	$1.25 \pm 0.43$	$6.15_{-0.39}^{+0.44}$
4b	...	15.7285033	-49.2541646	A	...	...	...	$2.85_{-0.36}^{+0.42}$
ALMA-b	...	15.7288345	-49.2540943	...	...	$296 \pm 124$	...	$2.53_{-0.39}^{+0.45}$
1c	4.3273	15.7123036	-49.2593173	...	$0.09 \pm 0.08$	$4.13 \pm 0.86$	$45.9 \pm 41.9$	$3.98_{-0.15}^{+0.15}$
2c	...	15.7134793	-49.2602988	...	$0.009 \pm 0.004$	$0.45 \pm 0.15$	$50.0 \pm 27.8$	$4.18_{-0.16}^{+0.16}$
3c	4.3289	15.7147336	-49.2606804	...	$1.10 \pm 0.56$	$1.62 \pm 0.34$	$1.47 \pm 0.87$	$4.36_{-0.18}^{+0.18}$
4c	...	15.7128864	-49.2607064	...	$0.92 \pm 0.23$	$4.40 \pm 0.94$	$4.78 \pm 1.53$	$4.13_{-0.17}^{+0.17}$
ALMA-c	...	15.7128881	-49.2608024	...	$58.1_{-30.7}^{+288.4}$	$201 \pm 84$	$3.46_{-3.12}^{+6.94}$	$4.18_{-0.17}^{+0.18}$

**Notes.** The coordinates and properties of the associated ALMA source are also listed in each case. Column 5 indicates whether Ly $\alpha$  is in emission (E) or only in absorption (A). The SFRs in column 7 have been obtained from the extinction-corrected, rest-UV flux of each galaxy, except for the ALMA source, for which the dust-obscured SFR has been derived with MAGPPHYS. All stellar masses (column 6) and SFRs (column 7) are corrected for lensing magnification (using column 9; Caminha et al. 2021).

<sup>a</sup> Source at very similar redshift to the others, but farther away, so their association with the main MUSE galaxy group (sources ID #1 to 4) is unclear.

<sup>b</sup> There is a sky line on top of the Lyman- $\alpha$  line in the MUSE spectrum of source 2, so it is unclear whether this line is only in absorption or has a component in emission.

We also independently derived star formation rates for all our galaxies using their extinction-corrected, rest-frame UV fluxes (based on the F105W filter photometry) and the corresponding Kennicutt (1998) formula. For sources ID #1,2,3 the SFR have a value of at most a few  $M_\odot \text{ yr}^{-1}$ . As for the stellar mass, the SFR of source ID #4 is more difficult to constrain, but we find that its value is between  $\sim 4.4$  and  $\sim 23.5 M_\odot \text{ yr}^{-1}$ .

For source ID #3, we can independently derive an SFR from the H $\alpha$  excess in the IRAC 3.6  $\mu\text{m}$  band. Following the methodology described in Caputi et al. (2017), we obtained  $(28.2 \pm 7.9)$  and  $(4.74 \pm 1.33) M_\odot \text{ yr}^{-1}$  for sources ID #3a and c, respectively (both values are corrected for magnification). These SFRs are significantly larger than those obtained from the rest-UV fluxes (Table 1). These differences suggest that the extinction correction derived from the SED fitting of this source is likely underestimated (a minor difference in the  $E(B-V)$  value would produce a significant change in the inferred intrinsic UV flux). Nevertheless, these higher SFRs derived from the H $\alpha$  line do not qualitatively change the classification of this source on the SFR versus  $M^*$  plane, as we discuss below.

All stellar masses and SFRs quoted in Table 1 have been corrected for lensing magnification. The error bars on the stellar masses and SFRs incorporate the lensing magnification errors in quadrature, but these are almost always a minor component of the total error budget in these quantities.

In Table 1 we also quote the specific SFR (sSFR) for our galaxies. This parameter has the important advantage of being basically independent of lensing magnification (this is strictly true assuming that the magnification is constant throughout a

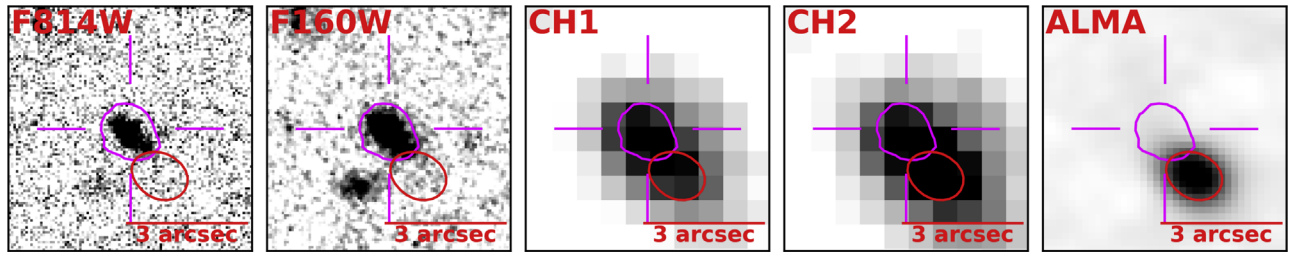
galaxy). Therefore the sSFR determination should be considered more robust than the SFR and stellar mass separately.

Figure 6 shows our MUSE group sources on the SFR versus  $M^*$  plane, along with other data points corresponding to lensed galaxies in other cluster fields and field galaxies, all at  $4 < z < 5$ . For reference, we also show the location of the star formation main sequence as well as starburst galaxies, as derived in previous works, albeit only for galaxies with stellar masses  $\gtrsim 10^8 - 10^9 M_\odot$  (Speagle et al. 2014; Caputi et al. 2017; Santini et al. 2017). Note that the starburst line in Figure 6 is the lower envelope of the starburst locus, defined by  $\log_{10}(\text{sSFR}(\text{yr}^{-1})) \geq -7.60$  (see Caputi et al. 2017).

From the location of our galaxies in this diagram we see that sources ID #3 and #4 can be classified as main-sequence galaxies. Interestingly, source ID #3 would still be classified as a main-sequence galaxy considering the SFRs inferred from the H $\alpha$  excess in the IRAC 3.6  $\mu\text{m}$  band. Sources ID #1 and #2, instead, lie above the starburst division line. Note, however, that we should take this classification with care because the main-sequence/starburst division is not known at stellar masses  $\lesssim 10^8 M_\odot$  and a linear extrapolation from higher stellar masses might not be strictly valid. In any case, the sSFR derived for sources ID #1 and #2 imply that the doubling time for their stellar masses is only  $2 \times 10^7 \text{ yr}$ , which is consistent with the short timescales expected for star formation episodes in local starburst galaxies (e.g., Knapen & James 2009).

None of the MUSE sources at  $z = 4.32$  is individually detected by ALMA, except for the association between the ALMA source discussed here and source MUSE ID #4. An ALMA stacking analysis of the MUSE group sources ID # 1, 2, and 3 in the three lensed components does not result in a signal either, as probably expected, indicating that the average





**Figure 3.** Postage stamps of MUSE source ID #4a and its associated ALMA detection. In all frames, the magenta and red contours show the MUSE and ALMA continuum emission regions, respectively.

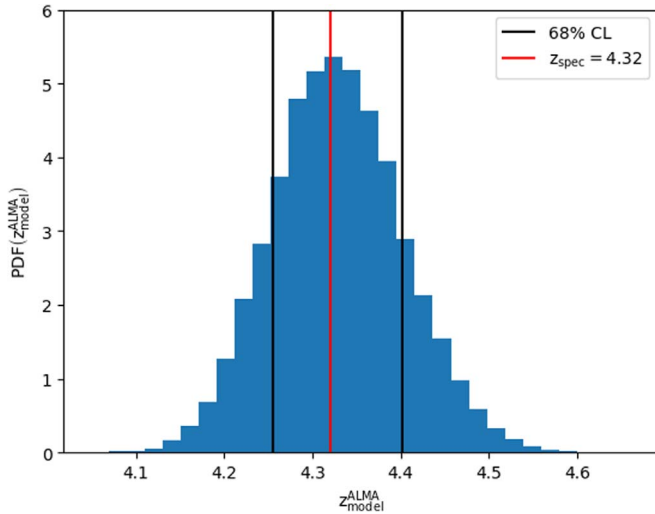


**Figure 4.** Probability density distribution of the ALMA source redshift based on lensing analysis (Caminha et al. 2021). This redshift distribution indicates that it is very likely that the ALMA source belongs to the same galaxy group as the MUSE galaxies at  $z = 4.32$ .

total infrared luminosity of these sources must be below a few  $\times 10^{10} L_{\odot}$  (after correcting for lensing magnification).

### 3.2.2. The Lensed ALMA Source

We also estimated the dust-obscured SFR for the ALMA source, using two different methods. In the first approach, we corrected the ALMA 1.2 mm flux densities for the lensing magnification in each component (see Table 1) and then we scaled them taking into account empirical sub-millimeter galaxy templates, following the same methodology as in Caputi et al. (2014). We obtained total infrared luminosities ranging between  $L_{\text{TIR}} = (1.23 \pm 0.52) \times 10^{12} L_{\odot}$  (component c) and  $(2.32 \pm 0.95) \times 10^{12} L_{\odot}$  (component b). Therefore, the ALMA source can be classified as an ordinary ultra-luminous infrared galaxy (ULIRG), with a luminosity more typical of the ULIRGs known at  $z = 2-3$  than the luminosities of the higher-redshift sub-/millimeter sources commonly studied in the pre-ALMA era. The derived SFRs using the Kennicutt (1998) formula corresponding to infrared luminosities are  $\text{SFR} \approx 130-250 M_{\odot} \text{yr}^{-1}$  ( $\pm 42\%$ ; after correction to a Chabrier IMF).

As a second, independent analysis, we considered the ALMA 1.2 mm flux densities, along with Herschel/SPIRE flux densities at 250, 350, and 500  $\mu\text{m}$  to perform the SED fitting of the ALMA source dust emission using the high- $z$  extension of the code MAGPHYS (Da Cunha et al. 2008). The Herschel detections are most secure for the ALMA source in component a (ALMA-a), for which the three SPIRE bands

yield a  $>3\sigma$  detection. ALMA-b was detected at  $3\sigma$  at 500  $\mu\text{m}$ , while ALMA-c was only detected above  $2\sigma$  at 350  $\mu\text{m}$ . In the case of non-detections, an upper limit of  $\sim 15$  mJy ( $3\sigma$ ) can be placed for their peak far-IR flux density in the SPIRE bands.

The output of the MAGPHYS SED fitting is consistent with our first total infrared luminosity estimates for the ALMA source. After correcting for lensing magnification, the values derived with MAGPHYS range between  $L_{\text{TIR}} = (1.86 \pm 0.89) \times 10^{12} L_{\odot}$  (component c) and  $(2.73 \pm 1.07) \times 10^{12} L_{\odot}$  (component b). These values correspond to dust-obscured SFRs ranging between  $\approx 200$  and  $300 M_{\odot} \text{yr}^{-1}$  ( $\pm 42\%$ ; after correction to a Chabrier IMF). These values are in reasonably good agreement with those obtained from our first estimation method for the total infrared luminosities.

We also estimated dust temperatures for these sources, following the methodology of Dudzevičiūtė et al. (2020). We obtained  $T_{\text{dust}} \approx 30.1-34.8$  K, which is consistent with the median temperature derived by Dudzevičiūtė et al. (2020) for sub-millimeter galaxies with  $L_{\text{TIR}} \sim 3.4 \times 10^{12} L_{\odot}$  at  $z \sim 2.5$ .

At wavelengths tracing the stellar emission, the ALMA source is only detected in the IRAC 3.6 and 4.5  $\mu\text{m}$  bands. Based on two secure data points, and HST flux upper limits, it would normally be difficult to do a proper SED fitting. However, in our case, we exploit the fact that we have an independent redshift determination for the ALMA source. We fit its SED running LEPHARE at the known fixed redshift to obtain an estimate of its stellar mass for two lensed components (see Figure 7 and Table 1). We obtained that the lensing corrected stellar mass of the ALMA source is between  $\sim 5.8$  and  $7.8 \times 10^{10} M_{\odot}$ . The stellar mass values obtained for the two lensed components are in a remarkably good agreement taking into that the SED fitting is mostly constrained by flux upper limits and that the IRAC photometry is somewhat blended with that of source ID #4.

With the SFR and stellar mass in hand, we can locate the ALMA galaxy on the SFR versus  $M^*$  plane (Figure 6). As is clear from this plot, the ALMA source is a main-sequence galaxy. Therefore, if MUSE source ID #4 and the ALMA source were two regions of the same galaxy, then the total system would still constitute a main-sequence galaxy.

## 4. Discussion

The existence of deep MUSE data on a lensing field reveals that the rather typical ALMA galaxy discussed in this paper is not alone. There are at least four star-forming galaxies associated with the ALMA source at  $z = 4.32$ , as confirmed by the three lensing components.

Previous works have shown that sub-/millimeter sources can trace active environments with multiple star-forming galaxies

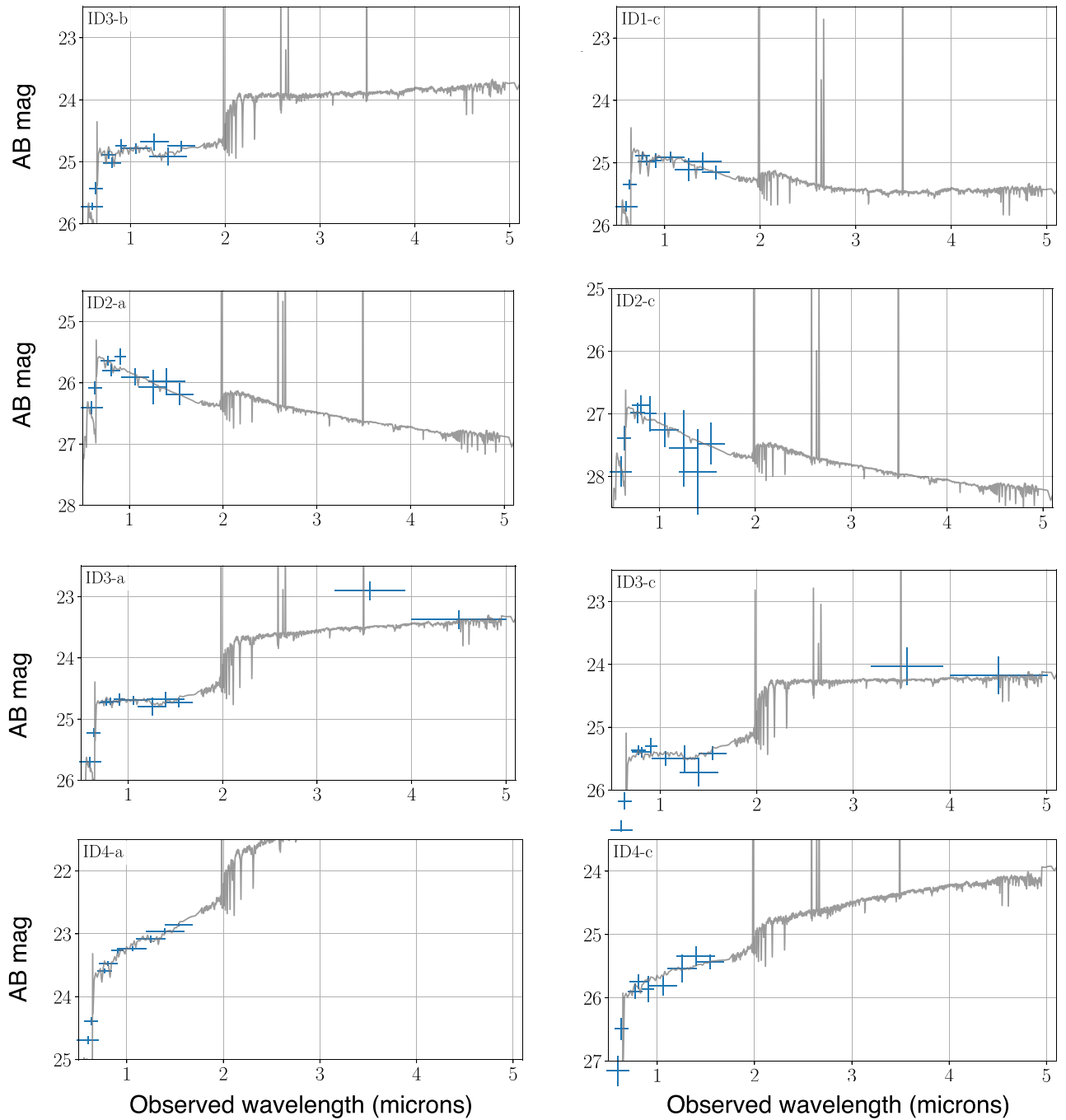


**Figure 5.** Best-fit SEDs for the four MUSE sources in the galaxy group at  $z = 4.32$ , in all the lensing components in which we have performed the SED fitting (those with photometry that is not significantly contaminated by the foreground cluster).

(e.g., Umehata et al. 2015; Miller et al. 2018; Oteo et al. 2018; Frye et al. 2019) and even be tracers of cosmic web filaments (e.g., Umehata et al. 2019). In most of these studies the system is dominated by an intrinsically bright sub-/millimeter galaxy. Gravitational lensing allows us to show that this property of tracing active environments is extended to less luminous systems. Kneib et al. (2004) reported a lensed galaxy group which includes an intrinsically sub-mJy sub-millimeter galaxy at  $z \sim 2.5$ . Here we report the discovery of another galaxy group of a similar kind, albeit much more compact and at a significantly higher redshift,  $z = 4.32$ .

The MUSE spectra, combined with the lensing effect, has been fundamental to this discovery. They provide the spectroscopic redshift confirmation for the group galaxies, as well as the necessary constraints for the lensing model to derive a secure redshift for the ALMA source and confirm its association with the MUSE galaxy group.

In spite of the dusty SFR derived for the ALMA source, which is much higher than the SFR of any other galaxy in the group, it is classified as a main-sequence galaxy on the SFR- $M^*$  plane. This should not be surprising, as other authors found that many high- $z$  sub-millimeter galaxies lie on the star formation main sequence (e.g., Michałowski et al. 2012; Schinnerer et al.

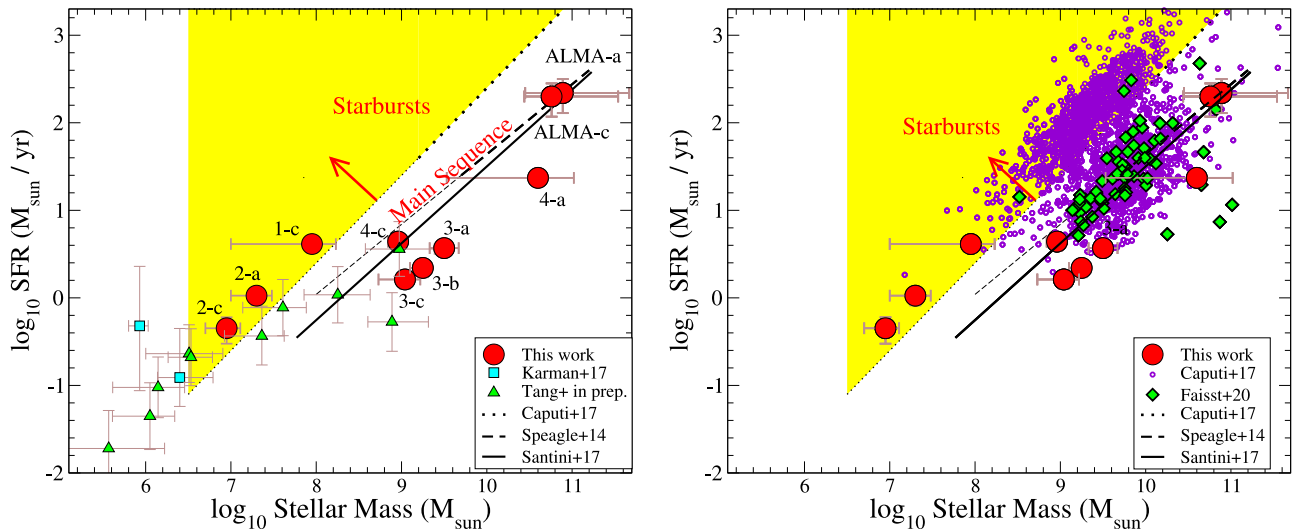


**Figure 6.** Location of our group sources on the SFR versus  $M^*$  plane, in comparison to other sources from the literature at redshifts  $4 < z < 5$ . Left: comparison to other lensed galaxies. Right: comparison to galaxies in the field, particularly prominent  $H\alpha$  emitters (Caputi et al. 2017) and ALMA galaxies (Faisst et al. 2020). In both panels, we indicate the average position of the star formation main sequence at the same redshifts, as obtained by Speagle et al. (2014; dashed-line) and Santini et al. (2017; solid line; determined by the analysis of lensing fields). The dotted line shows the lower envelope for the starburst classification at  $z \sim 4.3$  (Caputi et al. 2017). In all cases, thick lines are used for the stellar mass ranges in which these relations are known to be valid, while thin lines indicate linear extrapolations at lower stellar masses. For clarity, the source labels have been removed in the right panel.

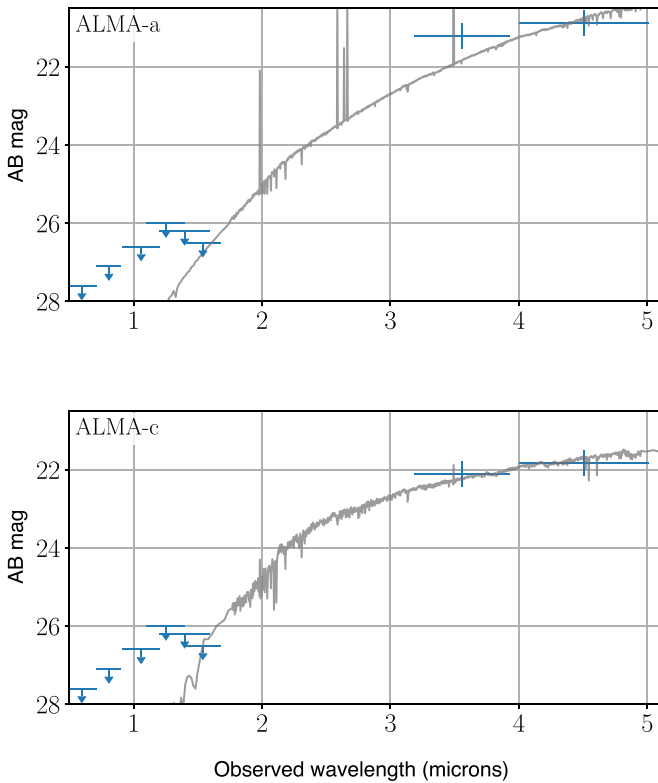


**Figure 7.** Best-fit SEDs for the ALMA source at  $z = 4.32$ , in the two lensing components in which we have performed the SED fitting.

2016; Lee et al. 2017; Michałowski et al. 2017; Schreiber et al. 2018). Source MUSE ID #4 is also classified as a main-sequence galaxy. If both sources were in fact regions of a single galaxy, the combination of both would still result in a main-sequence galaxy.

Although the derived SFRs of the MUSE sources are low in comparison with that of the ALMA source (in total they make for  $\sim 10\%$  of the ALMA galaxy SFR), in some cases these

SFRs are still relatively important taking into account the low stellar masses. Indeed, there are two starburst galaxies (ID #1 and #2) within the MUSE galaxy group. These two galaxies are expected to double their stellar masses in only  $2 \times 10^7$  yr, as derived from their sSFRs. Instead, MUSE source ID #3, like source ID #4, lies on the star-forming galaxy main sequence.

The classification of galaxies in the SFR versus  $M^*$  plane is poorly known for stellar masses  $\lesssim 10^9 M_\odot$ , as this region of parameter space is currently only constrained by a small amount of galaxies studied in lensed fields. We do not know whether the main-sequence/starburst classification, as it is usually defined at  $\gtrsim 10^9 M_\odot$ , is still valid at lower stellar masses. Nevertheless, we note that the statement that our MUSE sources ID #1 and #2 are starbursts is mainly based on their stellar mass doubling times, which is of only  $2 \times 10^7$  yr. These short timescales are similar to those characterizing star formation episodes in local starburst galaxies (Mihos & Hernquist 1994; Knapen & James 2009).

The presence of two starburst galaxies in this galaxy group with only 4–5 members makes for a starburst percentage of 40%–50%. Although this is based on very low statistics, this percentage is much higher than the overall starburst percentage known among star-forming galaxies at any redshift. This is perhaps not surprising taking into account the nature of our galaxy group. This is a compact galaxy group with a high velocity dispersion, in which the object interaction is likely triggering new star formation episodes. The effect is most drastic in the lowest mass galaxies, which is in line with the finding that the starburst fraction increases with decreasing stellar mass at different redshifts (Bisigello et al. 2018). It remains to be seen how ubiquitous these systems are, and if other similar systems also display such an enhanced fraction of starburst galaxies. Collecting statistically larger samples of these compact groups at different redshifts is necessary to draw a more general conclusion on this issue.

Based in part on observations carried out with ESO Telescopes at the Paranal Observatory under ESO program



ID 0102.A-0266. Also based on observations carried out by NASA/ESA Hubble Space Telescope, obtained and archived at the Space Telescope Science Institute. This paper makes use of the following ALMA data: ADS/JAO.ALMA#2018.1.00035.L. ALMA is a partnership of ESO (representing its member states), NSF (USA) and NINS (Japan), together with NRC (Canada), MOST and ASIAA (Taiwan), and KASI (Republic of Korea), in cooperation with the Republic of Chile. The Joint ALMA Observatory is operated by ESO, AUI/NRAO, and NAOJ.

We thank an anonymous referee for a constructive report. We thank Ian Smail for discussion on the paper. K.I.C., G.B.C., and S.D. acknowledge funding from the European Research Council through the award of the Consolidator Grant ID 681627-BUILDUP. K.K. acknowledges the support by JSPS KAKENHI grant No. JP17H06130 and the NAOJ ALMA Scientific Research grant No. 2017-06B. Y.A. acknowledges support by NSFC grant 11933011. K.K.K. acknowledges support from the Swedish Research Council and the Knut and Alice Wallenberg Foundation. C.G. acknowledges support through grant no.10123 of the Villum Fonden Young Investigator Programme. G.E.M. acknowledges the Villum Fonden research grant 13160 “Gas to stars, stars to dust: tracing star formation across cosmic time” and the Cosmic Dawn Center of Excellence funded by the Danish National Research Foundation under the grant No. 140. H.U. acknowledges support from JSPS KAKENHI grant (20H01953). E.V. acknowledges the financial support provided by the INAF for “interventi aggiuntivi a sostegno della ricerca di main-stream” Main-Stream (1.05.01.86.31).

*Facilities:* ALMA, VLT, HST, Spitzer, Herschel.

*Software:* SExtractor, IRAF, LePhare, MAGPHYS.

### ORCID iDs

K. I. Caputi <https://orcid.org/0000-0001-8183-1460>  
 G. B. Caminha <https://orcid.org/0000-0001-6052-3274>  
 S. Fujimoto <https://orcid.org/0000-0001-7201-5066>  
 K. Kohno <https://orcid.org/0000-0002-4052-2394>  
 Y. Ao <https://orcid.org/0000-0003-3139-2724>  
 L. Bradley <https://orcid.org/0000-0002-7908-9284>  
 D. Coe <https://orcid.org/0000-0001-7410-7669>  
 D. Espada <https://orcid.org/0000-0002-8726-7685>  
 C. Grillo <https://orcid.org/0000-0002-5926-7143>  
 B. Hatsukade <https://orcid.org/0000-0001-6469-8725>  
 K. K. Knudsen <https://orcid.org/0000-0002-7821-8873>  
 G. E. Magdis <https://orcid.org/0000-0002-4872-2294>  
 K. Morokuma-Matsui <https://orcid.org/0000-0003-3932-0952>  
 P. Oesch <https://orcid.org/0000-0001-5851-6649>  
 M. Ouchi <https://orcid.org/0000-0002-1049-6658>  
 H. Umehata <https://orcid.org/0000-0003-1937-0573>  
 F. Valentino <https://orcid.org/0000-0001-6477-4011>  
 E. Vanzella <https://orcid.org/0000-0002-5057-135X>  
 A. Zitrin <https://orcid.org/0000-0002-0350-4488>

### References

Arnouts, S., Cristiani, S., Moscardini, L., et al. 1999, *MNRAS*, 310, 540

Berciano Alba, A., Garrett, M. A., Koopmans, L. V. E., & Wucknitz, O. 2007, *A&A*, 462, 903  
 Bisigello, L., Caputi, K. I., Grogin, N., & Koekemoer, A. 2018, *A&A*, 609A, 82  
 Borys, C., Chapman, S., Donahue, M., et al. 2004, *MNRAS*, 352, 759  
 Bruzual, G., & Charlot, S. 2003, *MNRAS*, 344, 1000  
 Calzetti, D., Armus, L., Bohlin, R. C., et al. 2000, *ApJ*, 533, 682  
 Caminha, G. B., et al. 2021, *A&A*, submitted  
 Caminha, G. B., Karman, W., Rosati, P., et al. 2016, *A&A*, 595A, 100  
 Caputi, K. I., Deshmukh, S., Ashby, M. L. N., et al. 2017, *ApJ*, 849, 45  
 Caputi, K. I., Michałowski, M. J., Krips, M., et al. 2014, *ApJ*, 788, 126  
 Cerny, C., Sharon, K., Andrade-Santos, F., et al. 2018, *ApJ*, 859, 159  
 Chabrier, G. 2003, *PASP*, 115, 763  
 Chapman, S. C., Blain, A., Ibata, R., et al. 2009, *ApJ*, 691, 560  
 Chen, C.-C., Smail, I., Swinbank, A. M., et al. 2015, *ApJ*, 799, 194  
 Coe, D., Salmon, B., Bradač, M., et al. 2019, *ApJ*, 884, 85  
 Da Cunha, E., Charlot, S., & Elbaz, D. 2008, *MNRAS*, 388, 1595  
 Díaz, G. C., Ryan-Weber, E., Karman, W., et al. 2020, *MNRAS*, doi:10.1093/mnras/staa3129  
 Diego, J. M., Molnar, S., Cerny, C., et al. 2020, *ApJ*, 904, 106  
 Dudzevičiūtė, U., Smail, I., Swinbank, A. M., et al. 2020, *MNRAS*, 494, 3828  
 Egami, E., Rex, M., Rawle, T. D., et al. 2010, *A&A*, 518, L12  
 Faist, A. L., Schaerer, D., Lemaux, B. C., et al. 2020, *ApJS*, 247, 61  
 Fazio, G. G., Hora, J. L., Allen, L. E., et al. 2004, *ApJS*, 154, 10  
 Frye, B. L., Pascale, M., Qin, Y., et al. 2019, *ApJ*, 871, 51  
 Fujimoto, S., Ouchi, M., Ono, Y., et al. 2016, *ApJS*, 222, 1  
 Garrett, M. A., van der Werf, P. P., & Knudsen, K. K. 2005, *A&A*, 431, L21  
 Griffin, M. J., Abergel, A., Abreu, A., et al. 2010, *A&A*, 518, L3  
 Ilbert, O., Arnouts, S., McCracken, H. J., et al. 2006, *A&A*, 457, 8415  
 Karman, W., Caputi, K. I., Caminha, G. B., et al. 2017, *A&A*, 599A, 28  
 Karman, W., Caputi, K. I., Grillo, C., et al. 2015, *A&A*, 574, A11  
 Kennicutt, R. C., Jr. 1998, *ARA&A*, 36, 189  
 Knapen, J. H., & James, P. A. 2009, *ApJ*, 698, 1437  
 Kneib, J.-P., van der Werf, P. P., Knudsen, K. K., et al. 2004, *MNRAS*, 349, 1211  
 Lee, M. M., Tanaka, I., & Kawabe, R. 2017, *ApJ*, 842, 55  
 Lotz, J. M., Koekemoer, A., Coe, D., et al. 2017, *ApJ*, 837, 97  
 MacKenzie, T. P., Scott, D., Smail, I., et al. 2014, *MNRAS*, 445, 201  
 Martinache, C., Rettura, A., Dole, H., et al. 2018, *A&A*, 620A, 198  
 Menanteau, F., Hughes, J. P., Sifón, C., et al. 2012, *ApJ*, 748, 7  
 Michałowski, M. J., Dunlop, J. S., Cirasuolo, M., et al. 2012, *A&A*, 541A, 85  
 Michałowski, M. J., Dunlop, J. S., Koprowski, M. P., et al. 2017, *MNRAS*, 469, 492  
 Mihos, J. C., & Hernquist, L. 1994, *ApJL*, 431, L9  
 Miller, T. B., Chapman, S. C., Aravena, M., et al. 2018, *Natur*, 556, 469  
 Noeske, K., Weiner, B. J., Faber, S. M., et al. 2007, *ApJL*, 660, L43  
 Oke, J. B., & Gunn, J. E. 1983, *ApJ*, 266, 713  
 Oteo, I., Ivison, R. J., Dunne, L., et al. 2018, *ApJ*, 856, 72  
 Postman, M., Coe, D., Benítez, N., et al. 2012, *ApJS*, 199, 25  
 Rawle, T. D., Altieri, B., Egami, E., et al. 2016, *MNRAS*, 459, 1626  
 Riechers, D. A., Carilli, C. L., Capak, P. L., et al. 2014, *ApJ*, 796, 84  
 Rodighiero, G., Daddi, E., Baronchelli, I., et al. 2011, *ApJL*, 739, L40  
 Santini, P., Fontana, A., Castellano, M., et al. 2017, *ApJ*, 847, 76  
 Sargent, M. T., Béthermin, M., Daddi, E., & Elbaz, D. 2012, *ApJL*, 747, L31  
 Schinnerer, E., Groves, B., Sargent, M. T., et al. 2016, *ApJ*, 833, 112  
 Schreiber, C., Elbaz, D., Panella, M., et al. 2018, *A&A*, 609A, 30  
 Speagle, J. S., Steinhardt, C. L., Capak, P. L., & Silverman, J. D. 2014, *ApJS*, 214, 15  
 Umehata, H., Fumagalli, M., Smail, I., et al. 2019, *Sci*, 366, 97  
 Umehata, H., Tamura, Y., Kohno, K., et al. 2015, *ApJL*, 815, L8  
 Vanzella, E., Balestra, I., Gronke, M., et al. 2017a, *MNRAS*, 465, 3803  
 Vanzella, E., Calura, F., Meneghetti, M., et al. 2017b, *MNRAS*, 467, 4304  
 Weibacher, P. M., Streicher, O., Urrutia, T., et al. 2014, in ASP Conf. Ser. 485, *Astronomical Data Analysis Software and Systems XXIII*, ed. N. Manset & P. Forshay (San Francisco, CA: ASP), 451  
 Wu, J. F., Aguirre, P., Baker, A. J., et al. 2018, *ApJ*, 853, 195  
 Zitrin, A., Menanteau, F., Hughes, J. P., et al. 2013, *ApJL*, 770, L15